GEOPHYSICS, VOL. 76, NO. 1 (JANUARY-FEBRUARY 2011); P. F53–F63, 6 FIGS., 5 TABLES.
10.1190/1.3511356

Quantifying solute transport processes: Are chemically "conservative" tracers electrically conservative?

Kamini Singha[1], Li Li[2], Frederick D. Day-Lewis[3], and Aaron B. Regberg[4]

ABSTRACT

The concept of a nonreactive or conservative tracer, commonly invoked in investigations of solute transport, requires additional study in the context of electrical geophysical monitoring. Tracers that are commonly considered conservative may undergo reactive processes, such as ion exchange, thus changing the aqueous composition of the system. As a result, the measured electrical conductivity may reflect not only solute transport but also reactive processes. We have evaluated the impacts of ion exchange reactions, rate-limited mass transfer, and surface conduction on quantifying tracer mass, mean arrival time, and temporal variance in laboratory-scale column experiments. Numerical examples showed that (1) ion exchange can lead to resistivity-estimated tracer mass, velocity, and dispersivity that may be inaccurate; (2) mass transfer leads to an overestimate in the mobile tracer mass and an underestimate in velocity when using electrical methods; and (3) surface conductance does not notably affect estimated moments when high-concentration tracers are used, although this phenomenon may be important at low concentrations or in sediments with high and/or spatially variable cation-exchange capacity. In all cases, colocated groundwater concentration measurements are of high importance for interpreting geophysical data with respect to the controlling transport processes of interest.

INTRODUCTION

Tracer tests are commonly used in hydrogeology to investigate subsurface flow and transport processes. In numerous recent studies, electrically conductive tracers have been coupled with geophysical methods (e.g., Slater et al., 2000; French et al., 2002; Kemna et al., 2002; Vanderborght et al., 2005), which can provide spatially exhaustive maps with changes associated with the transport of the tracer. The goal of many of these studies has been to estimate spatial moments (e.g., mass, center of mass, and spatial variance) or temporal moments (e.g., mean arrival time) without many tens of wells being drilled for direct sampling (e.g., Binley et al., 2001; Singha and Gorelick, 2005; Day-Lewis et al., 2006; Looms et al., 2008). Although geophysical methods, such as electrical resistivity (ER) and ground-penetrating radar, can provide information about tracer breakthrough and preferential pathways that would be difficult and expensive to collect with conventional sampling, the treatment of geophysical data as surrogate hydrologic data is questionable in the presence of complex transport processes (e.g., bioremediation). The concept of a conservative tracer, commonly invoked in investigations of solute transport, requires additional study in the context of geophysical monitoring. For example, sodium chloride (NaCl) is a popular choice for tracer-test studies using geophysical methods given its low cost and small ionic radius, and it has been used at the field scale to image relative flow paths and barriers in numerous geological environments, from sand and gravel aquifers to fractured rock (e.g., Sidle et al., 1998; Day-Lewis et al., 2003; Levy and Berkowitz, 2003). It can be assumed that Cl^- is conservative and nonreactive, transporting along with groundwater, and thus analysis of NaCl tracer tests focuses on Cl^- (e.g., Harvey et al., 1989). Na^+, however, can go through reactive processes that would change concentrations of various species in the aqueous phase and therefore the ionic strength and fluid electrical conductivity of the system. Under these conditions, estimates of transport processes, such as velocities, that were made using methods sensitive only to electrical properties would be incorrect.

The exact relationship between ionic strength and fluid electrical conductivity has been debated in the literature (e.g., Reluy et al., 2004); however, this relationship is commonly found to be linear at the laboratory scale (e.g., Keller and Frischknecht, 1966; Mallants et

Manuscript received by the Editor 14 March 2010; revised manuscript received 7 July 2010; published online 4 January 2011.
[1]Pennsylvania State University, Department of Geosciences and Earth and Environmental Systems Institute, University Park, Pennsylvania, U.S.A. E-mail: ksingha@psu.edu.
[2]Pennsylvania State University, Department of Energy and Mining Engineering, University Park, Pennsylvania, U.S.A. E-mail: lili@eme.psu.edu.
[3]U. S. Geological Survey, Office of Groundwater, Branch of Geophysics, Storrs, Connecticut, U.S.A. E-mail: daylewis@usgs.gov.
[4]Pennsylvania State University, Department of Geosciences, University Park, Pennsylvania, U.S.A. E-mail: aregberg@psu.edu.

al., 1996). Fluid electrical conductivity can be described as a function of ionic strength:

$$\sigma_f = \frac{1}{2} F \sum_{j=1}^{n} u_j C_j |Z_j|, \quad (1)$$

where F is Faraday's constant (96,485 C/mol), C_j is the molar concentration of constituent ion j (mol/m^3), u_j is the electric mobility of ion j (m^2 V/s), Z_j is the charge of ion j (−), and j is the index of the n ions in solution (−). As shown by Kohlrausch's law of independent mobilities (Kohlrausch, 1897), the conductivity of the ions in solution is the sum of the conductivities for each ion when in dilute solution. Bulk electrical conductivity, measured via ER methods, is commonly thought to be a linear relationship of fluid electrical conductivity. For instance, Archie's law (Archie, 1942) indicates that

$$\sigma_b = n^q \sigma_f, \quad (2)$$

where σ_b is the bulk electrical conductivity (S/m); n is effective porosity; and q is the cementation exponent, which is related to connectivity of the pore space (Guyod, 1944). From equations 1 and 2, we see that the concentrations of aqueous species directly determine both the fluid and bulk electrical conductivity. For any aqueous solution with only monovalent anions and cations, the electrical neutrality of the soluble solution requires that equal numbers of the two ions are present. If the ions of interest are nonreactive, the measured fluid or bulk electrical conductivity directly characterizes the solute transport processes. However, some of the tracers that are commonly considered nonreactive and conservative may go through reactive processes, thus changing the aqueous composition of the system. As a result, the measured electrical conductivity may reflect not only transport but also reactive processes, which would be challenging to interpret from the geophysical signal without corroboratory chemical data.

One of the reactive processes that can affect concentrations of ionic tracers, such as Na^+, is ion exchange. Ion exchange is a reactive process that can control groundwater geochemistry (Appelo and Postma, 2005) and is particularly important in soils and aquifers that are rich in clay minerals (Valocchi et al., 1981; Appelo et al., 1993; Appelo, 1994; Grolimund et al., 1996; Vulava et al., 2002). Ion exchange has been found to control various processes, including saltwater intrusion (Lambrakis, 2006; Boluda-Botella et al., 2008), the migration of contaminants such as cesium and strontium (Lefevre et al., 1993; Steefel et al., 2003), and mineral precipitation (Harmsen and Bolt, 1982; Appelo, 1994). Depending on the relative concentration of relevant species, Na^+ is a species that is commonly involved in ion exchange reactions. Na^+ can exchange with other cation species, such as Mg^{2+}, Ca^{2+}, and K^+ on mineral surfaces, thereby altering aqueous geochemistry and the corresponding electrical properties. A representative exchange reaction between Na^+ and Ca^{2+} on a mineral surface can be written as follows:

$$Na^+ + 0.5CaX_2 \Leftrightarrow 0.5Ca^{2+} + NaX, \quad (3)$$

where NaX and CaX_2 represent the surface complexes that are formed between cations (Na^+ and Ca^{2+}, respectively) and mineral surface sites. Ion exchange reactions are reversible and occur quickly, and therefore they are often considered at equilibrium. Following the Gaines-Thomas convention, its equilibrium constant can be written as follows (Appelo and Postma, 2005):

$$K^G_{Na\backslash Ca} = \frac{[Ca^{2+}]^{0.5}[NaX]}{[Na^+][CaX_2]^{0.5}}, \quad (4)$$

where $[i]$ is the concentration or activity of species i in solution (Na^+ and Ca^{2+}), $[iX]$ is the concentration or activity on the exchanger surface, and $K^G_{Na\backslash Ca}$ is the equilibrium constant that is determined from the concentrations or activities of the involved species in aqueous and solid phases. As can be seen from the above equation with the exchange reaction, the concentration of Na^+ is determined by the equilibrium constant (the selectivity) and the relative concentration of Ca^{2+} and Na^+ in solution and on the mineral surface. Although ion exchange is largely a function of selectivity based on the charge and size of the ions, mass action also affects exchange. For instance, Na^+ is less favored by mineral surfaces than Ca^{2+} (Appelo and Postma, 2005); however, NaCl tracer tests commonly involve high concentrations — often g/L concentrations — such that Na^+ in solution can replace Ca^{2+} from the surface, thus changing the concentration of both Na^+ and Ca^{2+} in solution and on mineral surfaces. When high concentrations of ions exist, they may exchange and sorb at higher rates than expected based on selectivity alone (Ceazan et al., 1989). As such, the assumption that electrical conductivity and tracer concentration of a specific ion are directly and linearly related may not hold in many geologic or geochemical environments, such as materials with a high clay content.

Previous work has shown increased surface conductance associated with ions in solution exchanging with others on the grain surfaces and/or ions sorbing on charged surfaces (e.g., Leroy and Revil, 2004). In studies monitoring tracers, exchange processes would go undetected by geophysical methods sensitive to changes in electrical conductivity if the ionic strength remained constant. Although some research has considered using geophysical data to estimate cation exchange at the laboratory scale (Roberts and Lin, 1997), numerous other parameters (saturation, porosity, electrical properties of the ions) must be known, and these parameters vary greatly at the field scale and commonly cannot be measured. Cation exchange has been used to explain variability in field-scale electrical geophysical data (e.g., Ramirez et al., 1993; Singha and Gorelick, 2006), but limited or no chemical data exist to corroborate these assertions. Cation exchange is not commonly considered when imaging tracer transport with geophysical tools. We also note that although cation exchange is more common, anion exchange also occurs in the presence of low pH and iron or aluminum oxides, as seen in Boggs and Adams (1992).

Another process that can lead to complexities in interpreting geoelectrical data is rate-limited mass transfer (RLMT), where solutes diffuse in and out of dead-end pore space. RLMT may lead to a complex, time-varying relationship between electrical conductivity and tracer concentration (Singha et al., 2007, 2008; Day-Lewis and Singha, 2008). Singha et al. (2007) presented field-experimental data and numerical results suggesting that mass transfer has an observable geoelectrical signature. Experimental data collected during a push-pull freshwater injection into a brackish aquifer showed a hysteretic relationship between colocated measurements of bulk and fluid resistivity. For RLMT, a modified, bicontinuum version of Archie's law is instead used to estimate bulk conductivity from fluid conductivity in the mobile and immobile domains (Singha et al., 2007):

$$\sigma_b = (n_m + n_{im})^{q-1}(n_m\sigma_{f,m} + n_{im}\sigma_{f,im}), \quad (5)$$

where $\sigma_{f,m}$ is the mobile electrical conductivity at a given location (S/m), n_m is the mobile-domain porosity (−), n_{im} is the immobile-domain porosity (−), and $\sigma_{f,im}$ is the immobile electrical conductivity (S/m). According to equation 5, bulk conductivity is affected by both mobile and less-mobile solute. By contrast, conventional hydrologic sampling draws water preferentially from the mobile domain. Consequently, any estimate of solute transport behavior from ER data will be a function of the distribution of solute between domains and consequently not identical to processes that might be estimated from direct sampling.

Lastly, we consider a geophysical phenomenon, rather than a hydrologic process, and its implications for monitoring transport. Surface conductance may also affect the interpretation of geoelectrical data. Sediments with high cation exchange capacities (CECs), such as clay or shale-rich sediments, conduct current through the electrical double layer along mineral surfaces. Cations tend to concentrate near the surface of mineral grains to counterbalance the negative surface charge. A sample with high CEC will have a larger measured σ_b than a sample with a low CEC if all other variables (e.g., σ_f, porosity, tortuosity) are equal. Because additional conductivity from surface conductance results in the presence of sorbed ions or ions in the electrical double layer, equation 2 may underpredict bulk conductivity. Many different formulations for surface conductance exist (e.g., Waxman and Smits, 1968; Clavier et al., 1984; Revil and Glover, 1997); for example, consider the relatively simple relationship of Sen et al. (1988),

$$\sigma_b = n^q\left[\sigma_f + \frac{1.93qQ_v}{1 + 0.7/\sigma_f}\right]. \quad (6)$$

We note that this relationship looks similar to equation 2 with an additional term. Q_v is the counterion charge concentration (eq/L), which is directly related to the CEC (Revil et al., 1998):

$$Q_v \equiv \rho_g\frac{1-n}{n}CEC \quad (7)$$

where ρ_g is mineral grain density (g m^{-3}), and CEC is the cation-exchange capacity (meq g^{-1}). Surface conductance phenomena are most important at low ionic strength (<1 mM) (Revil et al., 1998). Other models for surface conduction (e.g., Leroy and Revil, 2004) address the electrochemical properties of clays more rigorously than the model shown in equation 7.

The assumption of a geophysically conservative tracer could be violated by numerous other processes (e.g., mineral dissolution and precipitation, sorption, or redox chemistry, depending on the tracer) or more complicated versions of the processes considered here (e.g., exchange of multiple ionic species, multirate mass transfer). We stress that our goal is not to present and demonstrate a comprehensive list of processes that may violate the assumption of a conservative tracer; rather, our goal is to bring to light this issue by presenting well-constrained models that may be used to support experiment design and interpretation. To investigate the effects of cation exchange, RLMT, and surface conductance on ionic strength and geoelectrical data, and the subsequent interpretation of hydrogeologic processes, we conducted synthetic experiments of tracer transport along 1D columns instrumented for direct-current electrical measurements. Although electrical measurements could be calculated analytically, we simulated electrical flow to account for any small errors introduced via discretization and 3D conduction and the finite size and geometry of electrodes, which are modeled as distributed sources and sinks rather than as point sources and sinks.

METHODS

We evaluated how estimates of mass, center of mass, and spatial variance would be affected by transport processes in the presence of ion-exchange reactions and those that involved mobile-immobile zones, and under what conditions the effects would be sufficient to affect electrical measurements. We also explored the effects of increased surface conductance. To these ends, we used (1) reactive transport modeling to simulate the transport and ion exchange processes, (2) electrical geophysical forward models to simulate bulk electrical resistivity measurements based on fluid conductivity, and (3) temporal moment analysis to quantify effects on transport.

Reactive transport simulation

We considered 1D solute transport involving advection, dispersion, and, in some cases, ion-exchange reactions or RLMT. We compared these models with one considering conservative, nonreactive Na^+ to investigate how these processes would affect our estimates of transport behavior.

The reactive transport system involves both ion exchange and aqueous speciation, as shown in Table 1. We include aqueous speciation reactions because they always occur; however, as will be shown in the Results section, they are not the dominant reactive process in our model system. Reactive transport models usually partition aqueous species into primary and secondary species, and the equations of mass conservation are written only for primary species (Lichtner, 1985; Steefel and Lasaga, 1994). For a system that involves both transport and ion exchange, the governing equations for the primary species have the following form:

$$\frac{\partial(nc_{T,i})}{\partial t} + \rho\frac{\partial(s_{T,i})}{\partial t} = \nabla\cdot(n\mathbf{D}\nabla c_{T,i}) - v\cdot\nabla(nc_{T,i}), \quad (8)$$

$$i = 1,2,\ldots,N_p,$$

where N_p is the total number of primary species; n is the total porosity, including both mobile and immobile porosity; $c_{T,i}$ is the total con-

Table 1. Geochemical reactions involved in the column.

Reaction	Log K_{eq}
Ion exchange reactions:	
$Na^+ + 0.5CaX_2 \Leftrightarrow 0.5Ca^{2+} + NaX$	−0.39[a] (Gaines-Thomas convention)
Aqueous speciation reactions:	
$CO_2(aq) + H_2O \Leftrightarrow H^+ + HCO_3^-$	−6.34
$HCO_3^- \Leftrightarrow H^+ + CO_3^{2-}$	−10.32
$CaHCO_3^+ \Leftrightarrow Ca^{2+} + HCO_3^-$	−10.43
$NaHCO_3(aq) \Leftrightarrow Na^+ + HCO_3^-$	−15.57
$H_2O \Leftrightarrow H^+ + OH^-$	−14.00

[a]Value from Appelo et al. (1993) and Appelo (1994).

centration of primary species i (solute mass/volume of pore water), defined as the summation of the concentration of primary species i and all secondary species that can be expressed in terms of the primary species i based on equilibrium relationships; ρ is the bulk density of the solid phase (mass of solid phase/volume of pore water); $s_{T,i}$ is the sorbed phase concentration of species i (solute mass/mass of solid phase); D is the hydrodynamic dispersion tensor (L^2/T); v is the pore water velocity (L/T); and t is time. Because of the local equilibrium assumption, the effects of ion exchange are implicitly embedded in the second term of the left side of the equation. For primary species that do not participate in ion-exchange reactions, the second term is zero. The reactive transport modeling code CrunchFlow (Steefel and Maher, 2010) was used to solve equation 8 for all primary species and then calculate the concentrations of secondary species.

Advective-dispersive transport with RLMT was described by two coupled partial differential equations, one for the mobile domain and one for the immobile domain:

$$n_m \frac{\partial c_m}{\partial t} + n_{im} \frac{\partial c_{im}}{\partial t} = \nabla \cdot (n_m \mathrm{D} \nabla c_m) - n_m v \cdot \nabla c_m, \quad (9a)$$

and

$$\frac{\partial c_{im}}{\partial t} = \alpha (c_m - c_{im}), \quad (9b)$$

where c_m is the mobile-domain concentration (M/L^3); c_{im} is the immobile-domain concentration (M/L^3); D is the hydrodynamic dispersion tensor (L^2/T); v is the pore water velocity (L/T); and α is the mass-transfer rate coefficient (T^{-1}). Solute movement between domains is represented here by simple first-order exchange (equation 9b), although more complicated models exist (Haggerty and Gorelick, 1995; Berkowitz et al., 2006). We solved equation 9 using the finite-difference simulation code MT3DMS (Zheng and Wang, 1999).

For either transport model, for each time step, electrical mobilities were calculated for each ion according to the Nernst-Einstein relationship for dilute solutions (Robinson and Stokes, 1959; Bockris and Reddy, 1998):

$$u_i = \frac{D_i Z_i F}{RT} \quad (10)$$

where D is the molecular diffusion coefficient in m^2/s for ion i, R is the molar gas constant equal to 8.31 J mol^{-1} K^{-1}, and T is the temperature in degrees Kelvin. Fluid conductivities were then calculated using equation 1 given the molar concentrations at every location.

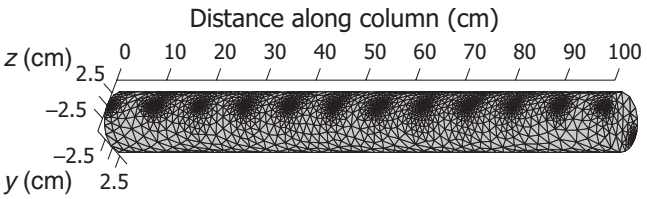

Figure 1. Image of column used for electrical forward modeling. The location of the 12 electrodes can be seen in the mesh; Wenner data were collected along these electrodes between neighboring electrodes. To create maps of electrical conductivity for this column, 1D transport simulations were converted to fluid electrical conductivity and then bulk electrical conductivity.

Electrical experiment simulation

Given the solute transport models above, we converted the concentration of solutes in the system to fluid conductivities using equation 1 and then to bulk electrical conductivity using equation 2, 5, or 6, depending on the conceptual model being tested, assuming a cementation exponent q of two, as seen in cemented materials (Keller and Frischknecht, 1966). In the case of a single-domain system with either a conservative or reactive tracer, equation 2 was used; for a dual-domain (RLMT) system, equation 5 was used, and if surface conductance was assumed to be an additional process (used here only with a single-domain system in the absence of ion exchange), equation 6 was used, assuming a Q_v of 1 meq/mL. Although other equations have been used to describe surface conductance, for the purpose of our demonstration, the simple relationship described by equation 6 was sufficient.

After the bulk conductivity was calculated, these values were input into a finite-element electrical model using the EIDORS toolbox (Adler and Lionheart, 2006) to simulate 3D DC electrical data. Values of bulk conductivity were assigned to 3D finite-elements by interpolating the 1D calculated fluid conductivities along the column (Figure 1). Electrodes were modeled as distributed sources/sinks with a geometry described by multiple finite elements comprising 0.5-cm square pads.

Temporal moments

The impacts of various physical and chemical processes (e.g., decay, mass transfer, dispersion) on overall solute-transport behavior are conveniently quantified using temporal moments (e.g., Harvey and Gorelick, 1995; Cunningham and Roberts, 1998; Cirpka and Kitanidis, 2000). Here, we performed temporal moment analysis for both the solute data and the electrical conductivity data. Temporal moments are given by

$$M_k(x) = n \int_\Gamma f(x) t^k dt, \quad (11)$$

where M_k is the kth temporal moment; k is an exponent with values 0–3, whose value depends on the particular moment of interest; n is the effective porosity; f is the change in fluid concentration C (or, in the case of the geophysical measurements, the electrical conductivity σ_f) from a background value; x is the Cartesian coordinate along the column; t is the time since the start of injection; and Γ is the test domain within the column of interest.

The zeroth moment M_0 is the mass in the system and is affected by decay or exchange reactions. The arrival time is given by the first moment (M_1) normalized by the mass, i.e., M_1/M_0, and is controlled by advective processes and retardation. The temporal variance of the tracer plume is related to the second temporal moment (M_2), mean arrival time, and tracer mass and is related to dispersion. The skewness of the concentration history is defined by moments up to order three and can be used to define tailing; a positive skew indicates a long tail arriving after the peak (e.g., Kreft and Zuber, 1978). Breakthrough curves that show early peaks or long tails indicate the possibility of preferential flow or RLMT. We considered moments up to order four, which allowed us to define the kurtosis, or peakedness, of our breakthroughs.

NUMERICAL EXAMPLES

We simulated the transport of an NaCl tracer through a 1D column initially filled with low-concentration $CaCl_2$. The tracer was introduced in a purge-type experiment, where the NaCl tracer was added continuously during the 200-day test from one end of the column. We first considered the behavior associated with (1) conservative transport and then explored cases with (2) ion exchange assuming local equilibrium, where Cl^- remains conservative but the Na^+ exchanges with Ca^{2+} in the host medium; (3) rate-limited mass transfer, where the ions in solution spend some time in disconnected porosity; and (4) time-varying surface conductance, where the ions sorb, creating additional surface conductance based on a simple model. We simulated flow and transport in a column 100 cm in length with a homogeneous hydraulic conductivity of 1 m/day and an effective porosity of 0.2. The finite-difference grid for flow and transport consisted of 1-cm cells. The inlet and outlet boundaries of the 1D column were held at a fixed flux to produce a specific discharge of 0.1 m/day. For all simulations, we assumed a dispersivity of 0.01 m, and we simulated transport of a tracer in the column over 200 days. The experimental design for column tracer tests is summarized in Table 2.

With respect to ion exchange, we simulated the transport of a 1 g/L NaCl tracer, a concentration seen in other tracer studies using geophysical methods, through a 1D column filled with a solution initially in equilibrium with calcite in a calcite-rich clayey formation. The sediment had a CEC of 120 meq/g, a typical value for soils and aquifers that contain some clay (Appelo et al., 1993; Appelo, 1994). The initial Ca^{2+} concentration was approximately 84.4 mg/L, and the initial solid phase Ca^{2+} was 5.90×10^{-5} meq/g solid. No diffusion was assumed. The pH of the column was assumed to be 8.0 at the start of the experiment, and the temperature was held at 25°C. Primary species in the simulations were Na^+, Ca^{2+}, Cl^-, HCO_3^-, and H^+. During the injection, Na^+ exchanged with some Ca^{2+} on the solid phase and therefore changed the aqueous concentrations of involved species. The initial geochemical conditions are shown in Table 3.

In a parallel column model ignoring ion exchange, RLMT was simulated using an identical column setup with MT3DMS (Zheng and Wang, 1999). In these models, we tracked total dissolved solids rather than specific chemical species. A mass transfer rate of 0.1/day was assumed, as was an immobile porosity of 0.2, giving a total porosity of 0.4. The system was otherwise similar to the conservative case.

Regardless of whether we considered conservative transport, ion exchange, or RLMT, we converted concentrations to fluid conductivity to bulk conductivity as previously outlined to simulate electrical flow. For the electrical measurement apparatus, we assumed a total of 12 electrodes arranged in one row along the top of the column (Figure 1). Electrodes were modeled as 0.5-cm square pads consisting of multiple elements. The finite-element mesh comprised 18,420 tetrahedral elements. Current injections involved the 12 electrodes in a skip-0 (e.g., Slater et al., 2000) Wenner configuration along the column. The resulting acquisition geometry consisted of only nine measurements for each time-lapse data set, which would take about 1 second to collect given current technology. Although only limited data are considered here, we made no attempt at image reconstruction but rather assessed the change in bulk measurements through time. These simulated electrical conductivity data sets were collected at a series of time steps — every half day at first, with spacing increasing over time — over the 200-day transport simulation. In the case where we introduced surface conductance, we built from the transport case considering conservative Na^+ for simplicity.

Table 2. Physical setup for synthetic column experiments.

Parameter	Value
Column length	100 cm
Specific discharge	0.1 m/day
Head gradient	0.01
Hydraulic conductivity, K	10 m/day
n_m	0.2
n_{im} (for RLMT case only)	0.2
Archie q	2

NUMERICAL MODELING

Reference case

As a reference case, we considered an NaCl tracer with no ion exchange, mass transfer, or surface conduction. In this case, the Na^+ displaced the Ca^{2+} and HCO_3^- in the column according to advective-dispersive transport (Figure 2). After four days, the column reached a new steady-state condition, dominated by Na^+ and Cl^-. In terms of the apparent bulk conductivity estimated from the forward simulation of electrical conduction, there was a predictable increase in electrical conductivity in the column with the introduction of the conservative tracer that mapped to an increase in fluid electrical conductivity (Figure 3a and e), and we found that moments estimated from the Cl^- concentration and the bulk conductivity matched closely (Figure 4). Although temporal moments for our purge-type experiment may have been less intuitive than for a pulse experiment, (1) purge experiments facilitated analysis of RLMT and other transport mechanisms (Day-Lewis and Singha, 2008), as there was no

Table 3. Initial geochemical conditions in the column.[a]

Species	Concentration (mol/L)
pH	8.0
Na^+	1.72×10^{-3}
Ca^{2+}	2.11×10^{-3} (in equilibrium with calcite)
HCO_3^-	5.68×10^{-4} (in equilibrium with atmospheric CO_2)
Cl^-	5.37×10^{-3}
Cation exchange capacity	1.20×10^{-4} eq/g solid phase
Na^+ on solid phase	1.99×10^{-6} meq/g solid
Ca^{2+} on solid phase	5.90×10^{-5} meq/g solid

[a]In the case of RLMT, no species were monitored directly. The concentration of total dissolved solids was assumed to be 100 mg/L as an initial condition, with a 1000 mg/L tracer introduced.

low-concentration tail as for pulse experiments, and (2) the differences in behavior between the conservative and reactive systems were clear in the moment analysis. The mass calculated from temporal moments decreased slightly along the column, which is indicative of nearly all of the mass that enters the column passing the outlet; some remnant tracer remained in the system after 200 days. The mean arrival time increased linearly along the column, as expected. The temporal variance and kurtosis decreased slightly along the column as a function of the movement of the NaCl step through the column in time. As demonstrated in this base case, ER can be used for conservative tracers to estimate tracer mass, mean arrival time, or the variance of the breakthrough, assuming that the ER electrode configuration is such that the method is sensitive to the changes in concentration (Table 4).

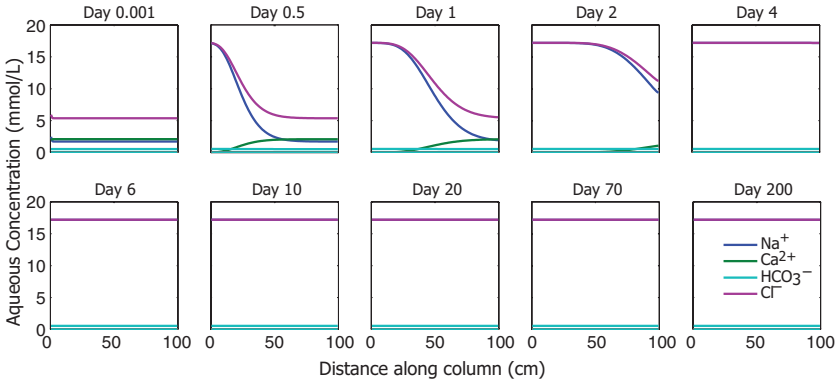

Figure 2. Aqueous concentration profiles associated with an NaCl tracer injected into a column originally filled with $CaCl_2$ solution and a carbonate-rich medium, assuming conservative transport. The concentrations of secondary species were too small to appear on these plots. Note that steady state was established by day 4.

Effect of ion exchange

In the presence of ion exchange, the NaCl tracer displaced the background $CaCl_2$ fluid, but the Na^+ also exchanged with the Ca^{2+} in the solid phase as the tracer migrated (Figure 5). Consequently, some of the Na^+ became absorbed to solid phase, and the aqueous concentration of Ca^{2+} increased as it was displaced by Na^+. As a result of ion exchange, Na^+ concentration decreased along the flow path, especially early in the experiment. Reactions occurring in the column are outlined in Table 1. Aqueous speciation reactions also occurred, with micromolar concentrations of $CaHCO_3^+$ and $CaCl^+$ also forming (not shown in

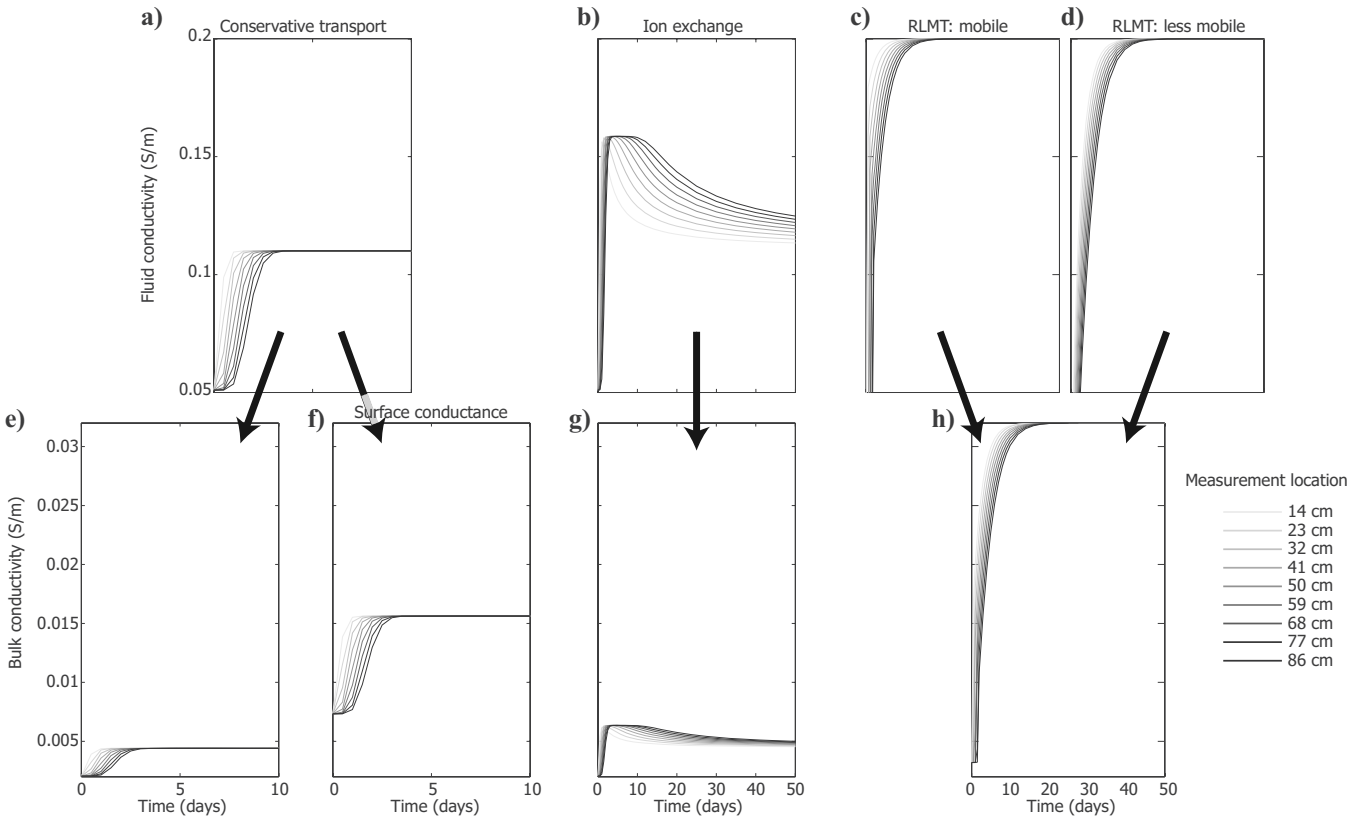

Figure 3. Fluid electrical conductivity for (a) conservative transport, (b) ion exchange, and (c and d) rate-limited mass transfer with time at nine locations in the column. Fluid conductivity measurements are pulled from a point location and based on transport simulations. The bottom row shows apparent bulk conductivity averaged over the column assuming four electrodes (two current, two potential) centered at the same location as the fluid sampling and based on electrical flow modeling; examples are shown for (e) conservative transport, (f) conservative transport in the presence of surface conductance, (g) ion exchange, and (h) rate-limited mass transfer based on the composite of the mobile and less-mobile concentrations. Note that the time axis is shorter on the conservative transport simulations due to the relative speed of transport behavior.

Figure 5 because concentrations were too low), indicating that these reactions were not the dominant reactive process.

With time, every location will be "saturated" with Na^+ on the grain surface and will not be able to adsorb more Na^+. This occurred first in locations close to the injection inlet. As a result, we saw an ion-exchange front that marked the highest concentration of Ca^{2+} and a corresponding low concentration of Na^+ that started from the inlet and moved gradually toward the outlet of the column. Eventually, after most of the sorbed Ca^{2+} was displaced from the solid phase, the spatial profiles would look exactly the same as those in the column without ion exchange.

Corresponding to the evolution of aqueous concentrations, we saw a substantial increase in fluid and apparent bulk electrical conductivity above the conservative case at early time points, with a subsequent return to the electrical conductivity expected from a conservative tracer on the order of 100 days, depending on the location of the quadripole along the column (Figure 3b and g). This overestimation of electrical conductivity and its latter stabilization at a lower level indicated that reactive transport was occurring. The exchange of Na^+ for Ca^{2+} in the column led to the additional increase in conductivity beyond that seen in the conservative test; hence, estimates of tracer concentration from electrical conductivity would be biased (overestimated), with the strength of the bias changing over the course of an experiment.

In the presence of ion exchange, we saw substantially different behavior in the ER than what would have been predicted by the tracer. The moments calculated from the ER indicated that the mass passing any point along the column increased near the outlet as a function of the changing ionic strength of the fluid, which is not physical (Figure 4). The estimates of higher-order moments led to unexpected results, as well. In the case of the mean arrival time, we found that breakthrough appeared to occur first in the outlet of the column and then migrating toward the inlet as a function of changing ionic strength, and the mean arrival time was notably lower in the presence of ion exchange than in the conservative case. The variance and kurtosis were also markedly high, resulting in errors as high as 7% (Table 4). These moments indicated that in the presence of reactive processes, ER-based estimates of solute transport processes may be incorrect.

Effect of rate-limited mass transfer

In the case of RLMT, we assumed that the mobile and less-mobile fractions of the aquifer were originally at equilibrium with 100 mg/L NaCl. Upon injection of the 1 g/L NaCl tracer, the solute moved preferentially through the connected pore space, with some fraction of the total concentration diffusing into a less-mobile domain at a fixed rate (here, equal to 0.1/day). After approximately 15 days of injection, the two domains came to equilibrium (Figure 6). The concentration moments based on rate-limited mass transfer (Figure 4) differed slightly — within approximately 1% — from the conservative case as a function of the fact that some of the solute in the mobile domain diffused into the less-mobile domain (Table 4). Consequently, more mass remained in the column after 200 days, solute mean arrival time was later along the column, and temporal variance and kurtosis were lower.

The lag between the mobile and less-mobile fluid conductivity was apparent in the ER data (Figure 3c and d). The bulk conductivity was higher than in the previous examples because of the increased total porosity; the fluid conductivities of both domains contributed (Figure 3h). For the ER analysis, we found that temporal moments of apparent bulk conductivity overestimated the arrival time and underestimated the temporal variance because they were affected by the concentration in the less-mobile domain (Figure 4); however, mass was closely matched. In the immobile domain, solute still affected bulk conductivity (equation 5) but became effectively invisible to conventional hydrologic sampling, which draws water preferentially from permeable and well-connected pore space.

Effect of surface conduction

The conceptual model that considers surface conductance uses the same concentration histories as the base case, which considers the conservative tracer shown in Figure 2. In this simulation, transport behaved identically to the conservative case, but additional bulk conductivity was present, as expected based on equation 6 (Figure 3f). The total ER-estimated mass in the system increased as a function of the additional conductivity; however, the velocity and dispersivity estimates were not affected (Table 4). In this example, surface conductance did not affect higher-order moments (Figure 4), because at high fluid electrical conductivity, the nonlinearity of the relationship between bulk and fluid conductivity was not substantial.

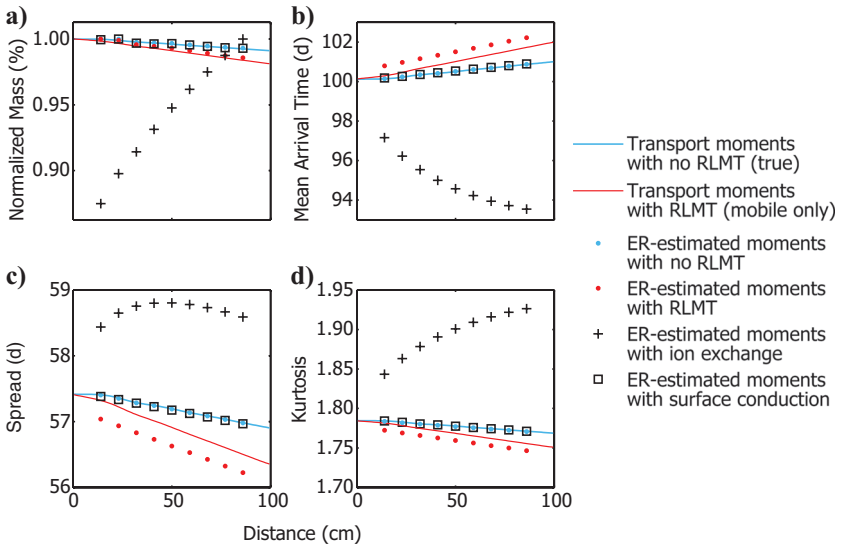

Figure 4. Temporal moments, including (a) normalized mass, (b) mean arrival time, (c) temporal variance, and (d) kurtosis estimated from NaCl tracer experiment and associated bulk apparent resistivity data for the four cases considered: conservative transport, ion exchange, RLMT, and surface conductance. Mass was normalized by the maximum value for each case so that values estimated from concentration could be plotted on the same axis as those based on apparent bulk electrical conductivity. Note that the moments estimated from ER for the conservative case and those in the presence of surface conductance lie on top of those estimated from the Cl^- tracer data for this experiment. The ER-estimated moments for the RLMT case are similar but not identical to what would be calculated by the mobile concentration; d indicates day.

For the surface-conduction model and example considered here, ER can still be used to estimate parameters controlling transport processes.

We note that introducing an ionic tracer decreased the effect of surface conduction in equation 6; the discrepancy between bulk conductivity estimated from equations 2 and 6 decreased as the fluid conductivity increased. Although not a major concern for the example shown here, the effect of the surface conductance will be higher for unsaturated media.

Table 4. Percentage error in transport characteristics of interest from the true conservative concentration data based on electrical conductivity measurements.

Plume characteristic	Simulation	Error with respect to true concentration (%)
Estimated mass	Conservative	0.043
	Ion exchange	5.5
	RLMT	0.33
	Surface conductance	0.048
Mean arrival time	Conservative	0.0058
	Ion exchange	5.6
	RLMT	1.0
	Surface conductance	0.030
Variance	Conservative	0.0059
	Ion exchange	2.6
	RLMT	0.98
	Surface conductance	0.030
Kurtosis	Conservative	0.0058
	Ion exchange	6.6
	RLMT	1.0
	Surface conductance	0.030

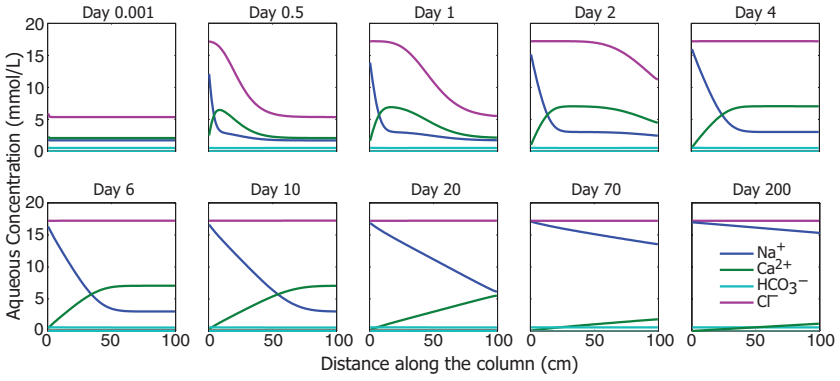

Figure 5. Concentration profiles associated with an NaCl tracer injected into a column originally filled with $CaCl_2$ solution and a carbonate-rich medium, assuming ion exchange. The concentrations of secondary species were too small to appear on these plots. Note that the system had not yet achieved a new steady state by day 100, meaning that there was Ca^{2+} on the solid phase that had not been displaced.

DISCUSSION

Through a series of numerical experiments, we have shown the following: (1) ion exchange can lead to ER estimates of tracer mass, velocity, and dispersivity that may be inaccurate; (2) mass transfer leads to a small overestimate in the mobile tracer mass and underestimate in velocity when using ER; and (3) surface conductance does not notably affect estimated moments given conditions with high fluid conductivity tracers under saturated conditions (Table 5).

Importantly, multiple studies have noted poor estimates of tracer mass from ER data (e.g., Binley et al., 2002; Singha and Gorelick, 2005) as a function of resolution (e.g., Day-Lewis et al., 2007). Here, we note that the apparent bulk resistivity values, which in this case are close to the true values, produce an estimate of tracer mass passing any particular location that will not be appropriate in any material that has high CEC; however, issues such as surface conductance and RLMT may not prohibit the use of geophysical methods to estimate groundwater velocities or tracer masses, assuming good data quality (and good resolution, in the case of inversion).

For instance, mass transfer processes are not always readily detectable, and they are a function of the flow velocity, length of tracer transit, and duration of the experiment (e.g., Haggerty et al., 2004). If the time scale of mass transfer is small relative to the time scale of advection, exchange between domains is so rapid that the mobile and less-mobile concentrations are near equilibrium. Similarly, for large time scales of mass transfer, the exchange between domains is so slow that breakthrough curves may be truncated prematurely depending on the experimental design, also leading to spurious estimates of moments. As a result, monitoring experiments need to be designed to achieve equivalent rates of advection and mass transfer, i.e., an experimental Damköhler number, DaI, of approximately 1:

$$DaI = \frac{\alpha(1 + n_{im}/n_m)L}{v} \tag{12}$$

where L is the domain length (Bahr and Rubin, 1987). Consequently, tracer experiments could be conducted that minimize the impact of processes such as RLMT by adjusting the pumping rate, for instance, thus maximizing the utility of electrical measurements for quantifying processes such as mean arrival time or temporal variance of the tracer.

Although surface conductance did not affect the estimation of transport processes in the synthetic column experiments conducted here, we assumed homogeneous lithology and a constant CEC of 120 meq/g across the length of the column. A constant CEC produces surface conductance that may have a negligible effect on electrical resistivity measurements; however, variability in this value is expected in most environmental systems. For example, many aquifers contain discrete areas of clay-rich sediment that would have locally elevated CEC. CEC also increases with increasing surface area, i.e., decreasing particle size (Revil et al., 1998). CEC also may vary as a function of pH (Langmuir, 1997), and thus surface conductance could vary temporally as well as spatially. For instance, as the tracer passes through zones of high CEC, bulk exchange ca-

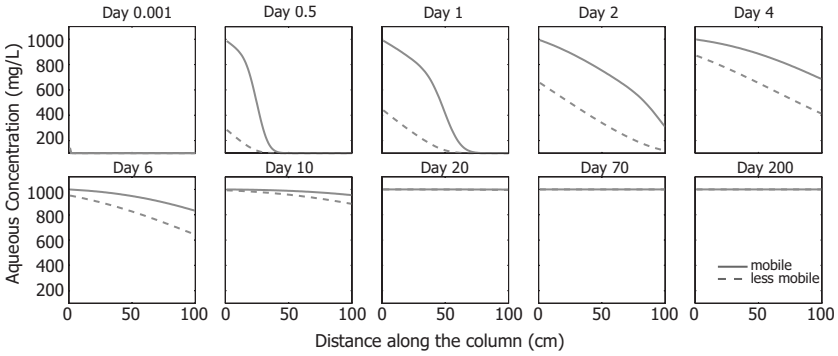

Figure 6. Concentration profiles associated with a conservative tracer of 1000 mg/L concentration injected into a column with a background of 100 mg/L total dissolved solids in the presence of rate-limited mass transfer. Note that the lag between mobile and less-mobile concentration disappeared by day 20.

Table 5. Effect of hydrogeochemical processes on fluid and bulk electrical conductivity compared with a conservative tracer.

Process	Effect on fluid conductivity	Effect on bulk conductivity
Ion exchange	Increase or decrease as a function of varying charge on ions in solution	Can appear to create or destroy mass due to changes in fluid conductivity; estimates of velocity and dispersivity may be poor
Rate-limited mass transfer	Different values in the connected and less-connected domains	Bulk is a composite of two domains; estimated velocities may be too slow
Time-varying surface conduction	None	Value is notably higher, but effect on moments is small for high concentration tracers

pacity would increase due to surface conductance only to decrease again as the tracer exited.

The examples here, in many ways, are a best-case scenario; the information content of the electrical data is high in this column experiment. With this in mind, we found that the ER measurements for the experiments presented here did an excellent job of matching most tracer moments if tracer transport was conservative or in the presence of surface conductance; however, RLMT led to small discrepancies on the order of 1%, and ion exchange led to more substantial discrepancies of 5 or 6% for most moments (Table 4). We note that the errors here were substantial, although small, and within the range of ER model variances. In the field, however, where poorer data quality will play a more substantial role, these errors will likely magnify. These results have implications for studies where time-lapse imaging is used to monitor biostimulation (Lane et al., 2006) or other remedial processes (Hubbard et al., 2008), where reactive transport may complicate interpretation of amendment concentration or geochemical conditions. Time-lapse images of tracer tests, injection experiments, and other dynamic processes may require interpretation in the context of reactive transport, RLMT, and/or surface conduction.

CONCLUSIONS

Geophysical methods have much to offer in hydrogeologic studies in terms of an inexpensive way to monitor tracer transport over a broad range of scales. In several studies, temporal (and/or spatial) moments of plumes have been calculated based on time-lapse tomograms, to infer tracer arrival time, dispersion, and other quantities of hydrologic interest. Underlying such work is the assumption that tracers that are conservative and nonreactive such that their geophysical signature can be directly related to transport processes. Here, we evaluated this assumption in the context of ion exchange reactions, rate-limited mass transfer, and surface conduction. The first two of these processes relate to transport phenomena, whereas the third is a geophysical phenomenon. We demonstrated here that a conservative tracer, such as NaCl, may not be conservative in a geophysical or a geochemical sense. Our results have important implications for studies in which time-lapse electrical imaging is used in combination with tracer experiments. First, ion exchange can lead to changes in aqueous composition of the system that correspond not only to transport but also to reactive processes. As a result, resistivity-estimated tracer mass, velocity, and dispersivity may be inaccurate. Second, mass transfer leads to an overestimate in the mobile tracer mass and an underestimate in velocity when using electrical methods. Third, surface conductance may not notably affect estimated moments when high concentration tracers are used, although this phenomenon may be important at low concentrations or in materials with high and/or variable CEC. Additional work is required to evaluate the importance of these processes on interpretation of tomograms in the context of field-scale experiments, where image resolution and estimation error may be poorer.

Other processes not considered here may also play a role, depending on the tracer used, such as sorption or redox chemistry; we also did not consider kinetics or multirate mass transfer, which could affect the relationship between fluid and bulk electrical conductivity. Although our goal was not to demonstrate the impact of every process under all conditions, it is clear that conservative tracers may not be conservative from both geochemical and geophysical perspectives. Our results underscore the need for colocated groundwater concentration measurements to facilitate interpretation of geophysical data for controlling transport processes, and they indicate that geophysical data need to be interpreted in light of these measurements for improved spatial and temporal interpolation between often limited chemical data.

ACKNOWLEDGMENTS

We thank Ty Ferre and two anonymous reviewers for thorough review comments on this manuscript, and we thank Rory Henderson and Jay Nolan for internal reviews of a draft manuscript. This material is based upon work supported by the National Science Foundation Grant EAR-0747629, Department of Energy Grants DE-FG02-08ER64520 and DE-SC0001773, and the U. S. Geological Survey Toxic Substances Hydrology Program.

REFERENCES

Adler, A., and W. R. B. Lionheart, 2006, Uses and abuses of EIDORS: An extensible software base for EIT: Physiological Measurement, **27**, S25–S42.

Appelo, C. A. J., 1994, Cation and proton-exchange, pH variations, and carbonate reactions in a freshening aquifer: Water Resources Research, **30**, 2793–2805.

Appelo, C. A. J., J. A. Hendriks, and M. Vanveldhuizen, 1993, Flushing factors and a sharp front solution for solute transport with multicomponent ion-exchange: Journal of Hydrology, **146**, 89–113.

Appelo, C. A. J., and D. Postma, 2005, Geochemistry, groundwater and pollution, 2nd ed.: A. A. Balkema.

Archie, G. E., 1942, The electrical resistivity log as an aid in determining some reservoir characteristics: Transactions of the American Institute of Mining, Metallurgical and Petroleum Engineers, **146**, 54–62.

Bahr, J. M., and J. Rubin, 1987, Direct comparison of kinetic and local equilibrium formulations for solute transport affected by surface reactions: Water Resources Research, **23**, 438–452.

Berkowitz, B., A. Cortis, M. Dentz, and H. Scher, 2006, Modeling non-Fickian transport in geological formations as a continuous time random walk: Reviews of Geophysics, **44**, RG2003.

Binley, A., G. Cassiani, R. Middleton, and P. Winship, 2002, Vadose zone flow model parameterisation using cross-borehole radar and resistivity imaging: Journal of Hydrology, **267**, 147–159.

Binley, A., P. Winship, R. Middleton, M. Pokar, and J. West, 2001, High-resolution characterization of vadose zone dynamics using cross-borehole radar: Water Resources Research, **37**, 2639–2652.

Bockris, J. O. M., and A. K. N. Reddy, 1998, Modern electrochemistry, Vol I: Ionics: Plenum Publishing Corp.

Boggs, J. M., and E. E. Adams, 1992, Field study of dispersion in a heterogeneous aquifer 4: Investigation of adsorption and sampling bias: Water Resources Research, **28**, 3325–3336.

Boluda-Botella, N., V. Gornis-Yagues, and F. Ruiz-Bevia, 2008, Influence of transport parameters and chemical properties of the sediment in experiments to measure reactive transport in seawater intrusion: Journal of Hydrology, **357**, 29–41.

Ceazan, M. L., E. M. Thurman, and R. L. Smith, 1989, Retardation of ammonium and potassium transport through a contaminated sand and gravel aquifer: The role of cation exchange: Environmental Science and Technology, **23**, 1402–1408.

Cirpka, O. A., and P. K. Kitanidis, 2000, Characterization of mixing and dilution in heterogeneous aquifers by means of local temporal moments: Water Resources Research, **36**, 1221–1236.

Clavier, C., G. Coates, and J. Dumanoir, 1984, Theoretical and experimental bases for the dual-water model for interpretation of shaly sands: SPE Journal, **24**, 153–168.

Cunningham, J. A., and P. V. Roberts, 1998, Use of temporal moments to investigate the effects of nonuniform grain-size distribution on the transport of sorbing solutes: Water Resources Research, **34**, 1415–1425.

Day-Lewis, F. D., Y. Chen, and K. Singha, 2007, Moment inference from tomograms: Geophysical Research Letters, **34**, L22404.

Day-Lewis, F. D., J. W. Lane Jr., and S. M. Gorelick, 2006, Combined interpretation of radar, hydraulic and tracer data from a fractured-rock aquifer near Mirror Lake, New Hampshire, USA: Hydrogeology Journal, **14**, 1–14.

Day-Lewis, F. D., J. W. Lane Jr., J. M. Harris, and S. M. Gorelick, 2003, Time-lapse imaging of saline-tracer transport in fractured rock using difference-attenuation tomography: Water Resources Research, **39**, 10-1–10-11.

Day-Lewis, F. D., and K. Singha, 2008, Geoelectrical inference of mass transfer parameters: Theoretical basis and numerical experiments: Water Resources Research, **44**, W05201.

French, H. K., C. Hardbattle, A. Binley, P. Winship, and L. Jakobsen, 2002, Monitoring snowmelt induced unsaturated flow and transport using electrical resistivity tomography: Journal of Hydrology, **267**, 273–284.

Grolimund, D., M. Borkovec, K. Barmettler, and H. Sticher, 1996, Colloid-facilitated transport of strongly sorbing contaminants in natural porous media: A laboratory column study: Environmental Science & Technology, **30**, 3118–3123.

Guyod, H., 1944, Fundamental data for the interpretation of electric logs: The Oil Weekly, **115**, 21–27.

Haggerty, R., and S. M. Gorelick, 1995, Multiple-rate mass transfer for modeling diffusion and surface reactions in media with pore-scale heterogeneity: Water Resources Research, **31**, 2383–2400.

Haggerty, R., C. F. Harvey, C. F. von Schwerin, and L. C. Meigs, 2004, What controls the apparent timescale of solute mass transfer in aquifers and soils? A comparison of experimental results: Water Resources Research, **40**, W01510.

Harmsen, K., and G. H. Bolt, 1982, Movement of ions in soil, I. Ion exchange and precipitation: Geoderma, **28**, 85–101.

Harvey, R. W., L. H. George, R. L. Smith, and D. R. LeBlanc, 1989, Transport of microspheres and indigenous bacteria through a sandy aquifer: Results of natural- and forced-gradient tracer experiments: Environmental Science and Technology, **23**, 51–56.

Harvey, C. F., and S. M. Gorelick, 1995, Temporal moment generating equations: Modeling transport and mass-transfer in heterogeneous aquifers: Water Resources Research, **31**, 1895–1911.

Hubbard, S. S., K. Williams, M. Conrad, B. Faybishenko, J. Peterson, P. Long, and T. Hazen, 2008, Geophysical monitoring of hydrological and biogeochemical transformations associated with Cr(VI) Biostimulation: Environmental Science and Technology, **42**, 3757–3765.

Keller, G. V., and F. C. Frischknecht, 1966, Electrical methods in geophysical prospecting: Pergamon Press.

Kemna, A., J. Vanderborght, B. Kulessa, and H. Vereecken, 2002, Imaging and characterisation of subsurface solute transport using electrical resistivity tomography (ERT) and equivalent transport models: Journal of Hydrology, **267**, 125–146.

Kohlrausch, F., 1897, Ueber concentrations-verschiebungen durch elecrolyse im innern von lösungen und lösungsgemischen: Annals of Physical Chemistry, **62**, 210–239.

Kreft, A., and A. Zuber, 1978, On the physical meaning of the dispersion equation and its solutions for different initial and boundary conditions: Chemical Engineering Science, **33**, 1471–1480.

Lambrakis, N., 2006, Multicomponent heterovalent chromatography in aquifers. Modelling salinization and freshening phenomena in field conditions: Journal of Hydrology, **323**, 230–243.

Lane, J. W. Jr., F. D. Day-Lewis, and C. C. Casey, 2006, Geophysical monitoring of field-scale vegetable oil injections for biostimulation: Ground Water, **44**, 430–443.

Langmuir, D., 1997, Aqueous environmental geochemistry, Prentice Hall.

Lefevre, F., M. Sardin, and D. Schweich, 1993, Migration of strontium in clayey and calcareous sandy soil — Precipitation and ion-exchange: Journal of Contaminant Hydrology, **13**, 215–229.

Leroy, P., and A. Revil, 2004, A triple-layer model of the surface electrochemical properties of clay minerals: Journal of Colloid and Interface Science, **270**, 371–380.

Levy, M., and B. Berkowitz, 2003, Measurement and analysis of non-Fickian dispersion in heterogeneous porous media: Journal of Contaminant Hydrology, **64**, 203–226, doi: 10.1016/S0169-7722(02)00204-8.

Lichtner, P. C., 1985, Continuum model for simultaenous chemical reactions and mass transport in hydrothermal systems: Geochimica et Cosmochimica Acta, **49**, 779–800.

Looms, M. C., K. H. Jensen, A. Binley, and L. Nielsen, 2008, Monitoring unsaturated flow and transport using cross-borehole geophysical methods: Vadose Zone Journal, **8**, 227–237.

Mallants, D. M., M. Vanclooster, N. Toride, J. Vanderborght, M. T. van Genuchten, and J. Feyen, 1996, Comparison of three methods of calibrate TDR for monitoring solute movement in unsaturated soil: Soil Science Society of America Journal, **60**, 747–754.

Ramirez, A., W. Daily, D. LaBrecque, E. Owen, and D. Chesnut, 1993, Monitoring an underground steam injection process using electrical resistance tomography: Water Resources Research, **29**, 73–87.

Reluy, F. V., J. M. de Paz Becares, R. D. Zapata Hernandez, and J. Sanchez Diaz, 2004, Development of an equation to relate electrical conductivity to soil and water salinity in a Mediterranean agricultural environment: Australian Journal of Soil Research, **42**, 381–388.

Revil, A., L. M. Cathles, S. Losh, and J. A. Nunn, 1998, Electrical conductivity in shaly sands with geophysical applications: Journal of Geophysical Research, **103**, 23925–23936.

Revil, A., and P. Glover, 1997, Theory of ionic-surface electrical conduction in porous media: Physical Review B, **55**, 1757–1773.

Roberts, J. J., and W. Lin, 1997, Electrical properties of partially saturated Topopah Spring tuff: Water distribution as a function of saturation: Water Resources Research, **33**, 577–587.

Robinson, R. A., and R. H. Stokes, 1959, Electrolyte solutions, 2nd ed.: Butterworths.

Sen, P. N., P. A. Goode, and A. Sibbitt, 1988, Electrical conduction in clay bearing sandstones at low and high salinities: Journal of Applied Physics, **63**, 4832–4840.

Sidle, C. R., B. Nilson, M. Hansen, and J. Frederica, 1998, Spatially varying hydraulic and solute transport characteristics of a fractured till determined by field tracer tests, Funen, Denmark: Water Resources Research, **34**, 2515–2527.

Singha, K., F. D. Day-Lewis, and J. W. Lane Jr., 2007, Geoelectrical evidence for bicontinuum transport in groundwater: Geophysical Research Letters, **34**, L12401.

Singha, K., and S. M. Gorelick, 2005, Saline tracer visualized with electrical resistivity tomography: Field scale moment analysis: Water Resources Research, **41**, W05023.

——–, 2006, Effects of spatially variable resolution on field-scale estimates of tracer concentration from electrical inversions using Archie's law: Geophysics, **71**, no. 3, G83–G91.

Singha, K., A. Pidlisecky, F. D. Day-Lewis, and M. N. Gooseff, 2008, Electrical characterization of non-Fickian transport in groundwater and hyporheic systems: Water Resources Research, **44**, W00D07.

Slater, L., A. M. Binley, W. Daily, and R. Johnson, 2000, Cross-hole electrical imaging of a controlled saline tracer injection: Journal of Applied Geophysics, **44**, 85–102.

Steefel, C. I., S. Carroll, P. Zhao, and S. Roberts, 2003, Cesium migration in Hanford sediment: A multisite cation exchange model based on laboratory transport experiments: Journal of Contaminant Hydrology, **67**, 219–246.

Steefel, C. I., and A. C. Lasaga, 1994, A coupled model for transport of multiple chemical species and kinetic precipitation/dissolution reactions with application to reactive flow in single phase hydrothermal systems: American Journal of Science, **294**, 529–592.

Steefel, C. I., and K. Maher, 2010, Water-rock interaction: A reactive transport approach, *in* E. H. Oelkers and J. Schott, eds., Thermodynamics and kinetics of water-rock interactions: Reviews in Mineralogy & Geochemistry, **70**, 485–532.

Valocchi, A. J., R. L. Street, and P. V. Roberts, 1981, Transport of ion-exchanging solutes in groundwater — Chromatographic theory and field simulation: Water Resources Research, **17**, 1517–1527.

Vanderborght, J., A. Kemna, H. Hardelauf, and H. Vereecken, 2005, Potential of electrical resistivity tomography to infer aquifer transport characteristics from tracer studies: A synthetic case study: Water Resources Research, **41**, W06013.

Vulava, V. M., R. Kretzschmar, K. Barmettler, A. Voegelin, D. Grolimund, and M. Borkovec, 2002, Cation competition in a natural subsurface material: Prediction of transport behavior: Water Resources Research, **38**, 1049.

Waxman, M. H., and L. J. M. Smits, 1968, Electrical conductivities in oil-bearing shaly sands: SPE Journal, **8**, 107–122.

Zheng, C., and P. P. Wang, 1999, MT3DMS: A modular three-dimensional multispecies model for simulation of advection, dispersion and chemical reactions of contaminants in groundwater systems: Documentation and user's guide: Contract Report SERDP-99-1: U. S. Army Engineer Research and Development Center.